Macromolecules

Article

Cite This: Macromolecules 2018, 51, 3088−3096

Structural Elucidation of Amorphous Photocatalytic Polymers from Dynamic Nuclear Polarization Enhanced Solid State NMR

Nick J. Brownbill,[†] Reiner Sebastian Sprick,[†,‡] Baltasar Bonillo,[†] Shane Pawsey,[§] Fabien Aussenac,[∥] Alistair J. Fielding,[⊥] Andrew I. Cooper,[†,‡] and Frédéric Blanc*[,†,#]

[†]Department of Chemistry, University of Liverpool, Crown Street, Liverpool, L69 7ZD, United Kingdom

[‡]Materials Innovation Factory, University of Liverpool, 51 Oxford Street, Liverpool, L7 3NY, United Kingdom

[§]Bruker BioSpin Corporation, 15 Fortune Drive, Billerica, Massachusetts 01821, United States

[∥]Bruker France, 34 rue de l'industrie, 67166 Wissembourg, France

[⊥]School of Pharmacy and Biomolecular Sciences, Liverpool John Moores University, Liverpool, L3 3AF, United Kingdom

[#]Stephenson Institute for Renewable Energy, University of Liverpool, Crown Street, Liverpool, L69 7ZD, United Kingdom

Supporting Information

ABSTRACT: Dynamic nuclear polarization (DNP) solid-state nuclear magnetic resonance (NMR) offers a recent approach to dramatically enhance NMR signals and has enabled detailed structural information to be obtained in a series of amorphous photocatalytic copolymers of alternating pyrene and benzene monomer units, the structures of which cannot be reliably established by other spectroscopic or analytical techniques. Large ^{13}C cross-polarization (CP) magic angle spinning (MAS) signal enhancements were obtained at high magnetic fields (9.4−14.1 T) and low temperature (110−120 K), permitting the acquisition of a ^{13}C INADEQUATE spectrum at natural abundance and facilitating complete spectral assignments, including when small amounts of specific monomers are present. The high ^{13}C signal-to-noise ratios obtained are harnessed to record quantitative multiple contact CP NMR data, used to determine the polymers' composition. This correlates well with the putative pyrene:benzene stoichiometry from the monomer feed ratio, enabling their structures to be understood.

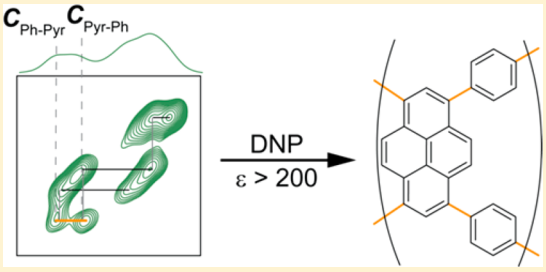

1. INTRODUCTION

Organic polymeric photocatalysts that generate hydrogen from water under electromagnetic irradiation have become an area of great interest in materials chemistry in recent years due to their potential greater diversity than classic metal based photocatalysts.[1−3] Organic photocatalysts such as graphitic carbon nitride[4] and poly(*p*-phenylenes)[5−7] are primarily active when irradiated with light in the UV region of the electromagnetic spectrum (just 3% of the solar light on the Earth's surface).[8] Recent developments in the field have targeted polymers active in the visible light region, the predominant wavelengths of radiation present in solar light, with tunable band gaps to optimize photocatalytic activity.[7−17]

One of these families of polymers (Figure 1), which belongs to the conjugated microporous polymers (CMPs),[18] is specifically investigated in this work due to both their remarkable hydrogen evolution rates under visible light (Figure 1) and their large accessible surface areas (Brunauer−Emmett−Teller surface areas (SA_{BET}) up to ∼1200 m^2 g^{-1}, Table S1, pore size distributions, Figure S1). These CMPs, known as copolymerized conjugated microporous polymers (CP-CMPs) are extended three-dimensional networks composed of copolymerized alternating pyrene and benzene monomer units in varying ratios to form multicomponent systems (Figure 1). They are both insoluble and amorphous, making their atomic level structure very challenging or impossible to obtain using standard analytical methods such as X-ray diffraction (Figure S2) or solution-state NMR. CP-CMPs' insolubility also prevents their physical properties such as particle size from being determined by chromatography-based techniques such as size exclusion or gel permeation chromatography. It is possible to empirically optimize photocatalytic activity of these materials; however, a targeted synthetic approach relies on the obtained polymer structure which cannot be assumed to be identical to the monomers input. The development of a robust method of characterization of CP-CMPs is vital to determining their compositions, and understanding and improving upon their remarkable activities.

Solid-state NMR spectroscopy is a well-established technique for short-range structure determination and has played an important role in elucidating extended polymer networks.[19,20] Nevertheless, the acquisition of quantitative directly excited ^{13}C spectra for these systems can be time-consuming as they are often multicomponent, containing repeat units at a low relative

Received: November 30, 2017
Revised: March 23, 2018
Published: April 10, 2018

DOI: 10.1021/acs.macromol.7b02544
Macromolecules 2018, 51, 3088−3096

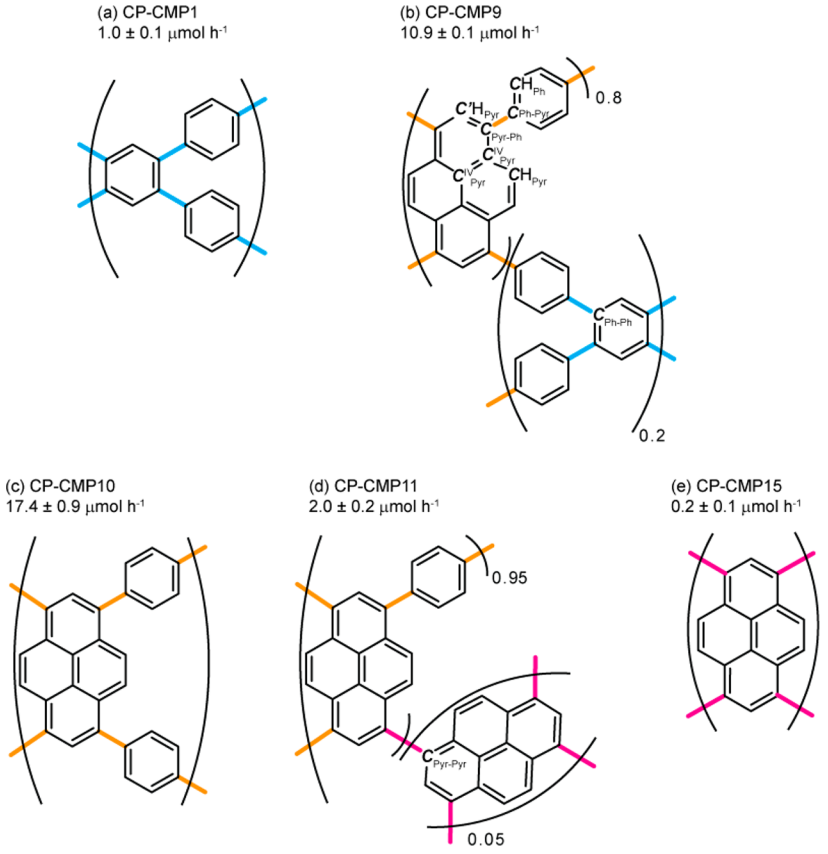

Figure 1. Putative structures of the copolymerized conjugated microporous polymers (CP-CMPs) studied here with compositions based on monomer feed ratio (Table 1). The photocatalytic hydrogen evolution rates for 100 mg polymer in water containing 20 vol % diethylamine as an electron donor under visible light (λ > 420 nm from a 300 W xenon light source) are displayed below each name. In parts b and d, each unique ^{13}C environment resolvable by NMR (see below) has been attributed a name within the structure. The bracketed sections represent randomly distributed minor components. The $C_{Pyr\text{-}Ph}$−$C_{Ph\text{-}Pyr}$ bonds that confirm copolymerization are given in orange, while homocoupling bonds of benzene and pyrene units are shown in cyan and magenta, respectively.

concentration[7,21−23] which can lead to their signals being obscured by higher intensity peaks and/or difficult to differentiate from baseline noise, and the ^{13}C spin−lattice relaxation times T_1 could be long. Although, Hartmann−Hahn cross-polarization[24] (CP) improves signal-to-noise ratio and time efficiency, this approach often requires substantial experimental times (hours)[19,20] and unlike direct ^{13}C excitation, CP spectra obtained with a single contact time only provide qualitative data, making the experiment redundant when quantification of ^{13}C signals is needed.

High field dynamic nuclear polarization (DNP)[25−28] is an emerging technology for enhancing solid-state NMR signals by multiple orders of magnitude, by transferring the large polarization of unpaired electrons to nuclei in close proximity to the electron source, with the hyperpolarization spreading between nuclei by spin diffusion before detection of the enhanced NMR signals. DNP has a long history of application to polymers such as polystyrene and polycarbonate derivatives[29−33] to enhance signal sufficiently to observe interfaces between domains within blended polymers. When combined with magic angle spinning (MAS) and ^{13}C CP,[34] this indirect DNP approach has been demonstrated as an extremely versatile technique for the characterization of polymers,[35−44] substantially reducing experimental times for microporous materials and delivering high throughput capability to solid-state NMR.[42] Nevertheless, quantification of the ^{13}C NMR resonances is still hampered by the nonquantitative nature of CP (*vide supra*). Note that direct DNP (electron-^{13}C polarization transfer without ^{1}H polarization and CP step) is not quantitative due to the lack of spin diffusion to distribute the hyperpolarization in these systems.[45] A quantitative approach to CP known as multiCP was first reported in 1990[46] and consists of multiple short CP contact pulses, separated by delays long enough for substantial ^{1}H longitudinal relaxation but with minimal ^{13}C relaxation leading to cumulative polarization with each short contact pulse (the pulse program is shown in Figure S3d). MultiCP has recently regained popularity[47−52] to provide time efficient quantification of organic matter and materials such as pharmaceutical excipients and metal organic frameworks. This approach, when combined with DNP enhanced ^{13}C MAS NMR, provides an appealing route to obtain quantitative NMR spectra quickly and is explored here to determine the compositions of photocatalytically active CP-CMPs (Figure 1).

Here we demonstrate that DNP represents a time efficient approach to obtain high signal-to-noise ^{13}C NMR spectra of CP-CMPs. We show that the high signal obtained facilitates the acquisition of a two-dimensional ^{13}C−^{13}C through-bond correlation spectrum at natural abundance of amorphous macromolecules; such a spectrum could not be obtained without DNP. Enhancement values of up to $\varepsilon_{C\ CP}$ > 200 at 9.4 T are possible via the cross effect (CE) DNP mechanism,[53] allowing the ^{13}C NMR spectra of the series of polymers to be obtained quickly (hours) and which enables tracking minor changes in the polymeric structure. Combining these large

DOI: 10.1021/acs.macromol.7b02544
Macromolecules 2018, 51, 3088−3096

DNP enhancements with the quantitative multiCP experiment,[49] we were able to determine the polymers' compositions, estimate the average polymeric structure and compare with the monomer feed ratio, a result that cannot be obtained by any other spectroscopic or analytical method.

2. EXPERIMENTAL PROCEDURES

Materials Synthesis. All CP-CMPs were synthesized according to a previously published procedure.[8] In brief, a library of polymers was synthesized by a Pd(0)-catalyzed Suzuki−Miyaura polycondensation[54] reaction of varying ratios of four monomers; 1,4-benzene diboronic acid (**M1**), 1,2,4,5-tetrabromobenzene (**M2**), 1,3,6,8-tetraboronic pinacol ester of pyrene (**M3**) and 1,3,6,8-tetrabromopyrene (**M4**) to yield pyrene/benzene copolymers of different compositions (Table 1).

Table 1. Relative Molar Monomer Feed Ratios of Each Polymer, with Monomers Defined in the Materials Synthesis Section

	relative molar monomer ratio			
copolymer	M1	M2	M3	M4
CP-CMP1	2	1	0	0
CP-CMP9	2	0.2	0	0.8
CP-CMP10	2	0	0	1
CP-CMP11	1.9	0	0.05	1
CP-CMP15	0	0	1	1

NMR Procedures. For DNP, incipient wetness impregnation, slurry, and dried preparations were all used. For incipient wetness impregnation (used unless stated otherwise), a preweighed amount of CP-CMP powder (typically around 10 mg) was impregnated with 80 μL of 20 mM TEKPol biradical[55] in 1,1,2,2-tetrachloroethane (TCE),[56] until the powder appeared saturated with the solution, and was then mixed uniformly. Slurries were prepared with ∼10 mg of polymer, which was mixed homogeneously with 120 μL of 20 mM TEKPol in TCE. In the dried preparation ∼10 mg of polymer was homogeneously mixed with 50 μL of 20 mM TEKPol in TCE and was then left to dry for 48 h, allowing all of the solvent to evaporate. The CP-CMP/TEKPol/TCE mixtures were then packed directly into 3.2 mm sapphire rotors and sealed with zirconia caps. Where stated, the samples were freeze/thaw cycled five times to remove paramagnetic oxygen from the matrix (Figure S4).[40,57]

DNP spectra at 600 MHz were recorded on a commercial 14.1 T Bruker Avance III DNP solid-state NMR spectrometer equipped with a 395.20 GHz gyrotron microwave system.[58] Experiments were recorded with a 3.2 mm HXY triple-resonance MAS probe at $\nu_0(^1H)$ = 600.084 MHz corresponding to the maximum enhancement ^1H position ε_H for binitroxide radical TOTAPOL[59] at $\nu_0(e^-)$ = 395.20 GHz, with the X channel tuned to ^{13}C at $\nu_0(^{13}C)$ = 150.91 MHz. All experiments were performed under magic angle spinning (MAS) at ν_r = 12.5 kHz and $T \approx 120$ K, as determined by spin−lattice relaxation times (T_1) measurements of ^{79}Br on a very small amount of KBr added to rotor.[60] All ^1H pulses and SPINAL-64 heteronuclear decoupling[61] were performed at a radio frequency (rf) field amplitude of 100 kHz. All ^{13}C CP MAS experiments were obtained with a ^{13}C rf field of 72 kHz, while the ^1H rf field amplitude was ramped to obtain maximum signal at a ^1H rf field of approximately 100 kHz. CP contact times were optimized for maximum signal on each polymer.

All DNP NMR experiments at 400 MHz were performed on a commercial 9.4 T Bruker Avance III DNP solid-state NMR spectrometer equipped with a 263.715 GHz gyrotron microwave system.[62] Experiments were recorded with a 3.2 mm HXY triple-resonance MAS probe at $\nu_0(^1H)$ = 400.07 MHz corresponding to the maximum enhancement ^1H position ε_H for TOTAPOL at $\nu_0(e^-)$ = 263.715 GHz, with the X channel tuned to ^{13}C at $\nu_0(^{13}C)$ = 100.61 MHz and at $T \approx 110$ K as above.[60] All ^{13}C CP MAS experiments were obtained with a ^{13}C rf field of 54 kHz, and all other parameters matched those at 600 MHz DNP. The INADEQUATE spectrum was recorded with ^{13}C rf field amplitude of 100 kHz, contact pulses at 90 kHz, while the ^1H rf field amplitude was ramped to obtain maximum signal at a ^1H rf field of approximately 100 kHz. A double quantum coherence delay of 3.4 ms was optimized, with a z-filter delay of 1.4 ms. All spectra were obtained with a recycle delay of a 1.3 × $\tau_{DNP}(^1H)$ for optimal signal-to-noise per unit time.[63]

All multiCP experiments were run with a 5 × $\tau_{DNP}(^1H)$ recycle delay, and 2 × $\tau_{DNP}(^1H)$ delays between contact pulses where $\tau_{DNP}(^1H)$ is the DNP polarization buildup times (see Figure S3d, and section S5 in the Supporting Information). Contact pulses of 1 ms were used with the exception of the final contact, which was 0.8 ms in duration, and number of pulses optimized for each polymeric system ranging from 6 to 10 repeats, and 8 scans were accumulated. All multiCP spectra were fitted using the sola function in Topspin 3.5 including ^{13}C CSA.

All standard solid-state NMR experiments were performed on a commercial 9.4 T Bruker Avance III HD solid-state NMR spectrometer equipped with a 4 mm HXY triple-resonance MAS probe (in double resonance mode) with the ^1H Channel tuned to ^1H at $\nu_0(^1H)$ = 400.13 MHz and the X channel was tuned to ^{13}C at $\nu_0(^{13}C)$ = 100.67 MHz. All experiments were performed under MAS at ν_r = 12.5 kHz and T = 298 K. All ^1H pulses and SPINAL-64 heteronuclear decoupling[61] were performed at an rf field amplitude of 83 kHz. All ^{13}C CP MAS experiments were obtained with a ^{13}C rf field of 45 kHz, while the ^1H rf field amplitude was ramped to obtain maximum signal at a ^1H rf field of approximately 60 kHz, and a contact time of 2 ms.

In all cases, T_1 and τ_{DNP} were obtained using saturation recovery experiments (Figure S3(a)). NMR data were obtained and analyzed using TopSpin 3.2, and all ^1H and ^{13}C spectra were referenced to H_2O at 4.8 ppm and the tertiary ^{13}C on adamantane at 29.45 ppm (corresponds to TMS at 0 ppm),[64] respectively. The chemical shifts of all assigned peaks are quoted within a realistic accuracy of ±1 ppm due to the broad line widths.

EPR Experiments. The 9 GHz (X band) continuous-wave electron paramagnetic resonance (EPR) spectra were recorded on a Bruker Biospin EMX spectrometer fitted with an Oxford Instruments ESR900 cryostat. At room temperature the spectra were obtained with 1 mW microwave power and 0.5 G modulation under nonsaturating conditions. At 120 K the spectra were obtained with 0.02 mW microwave power and 0.5 G modulation. The samples used were those prepared in the NMR section above and packed into capillary tubes, or standard EPR tubes.

EPR spin-counting experiments were recorded on an X-band Bruker Biospin EMX Nano spectrometer operating at 9.6 GHz and at room temperature. Samples were packed into 3.2 mm sapphire NMR rotors and sealed with zirconia caps. Spin counting calculations were performed as per the Bruker Spin Counting Manual procedure. The error on the spin counting measurements was determined to be ±10% while the determination of the electron concentration had an estimated error of approximately ±60% (due to the rapid evaporation of TCE during the sample packing procedure).

Powder X-ray Diffraction Measurements. Powder X-ray diffraction (PXRD) data (Figure S2) were collected in high throughput transmission mode on a Panalytical Empyrean diffractometer producing Cu Kα (λ = 1.5418 Å) radiation, equipped with an X-ray focusing mirror and PIXcel 3D detector.

Pore Size and Surface Area Measurements. The materials were degassed at 120 °C for 900 min under dynamic vacuum (10^{-5} bar) before analysis. Nitrogen adsorption and desorption isotherms were collected at 77.3 K using an ASAP2420 volumetric adsorption analyzer (Micromeritics Instrument Corporation). Brunauer−Emmett−Teller surface areas (SA_{BET}) were calculated in the relative pressure (P/P_0) range of 0.05−0.25. Pillared clay method of nonlocal density functional theory (NL-DFT) was used to determine the pore size distribution assuming a cylindrical pore geometry.

DOI: 10.1021/acs.macromol.7b02544
Macromolecules 2018, 51, 3088−3096

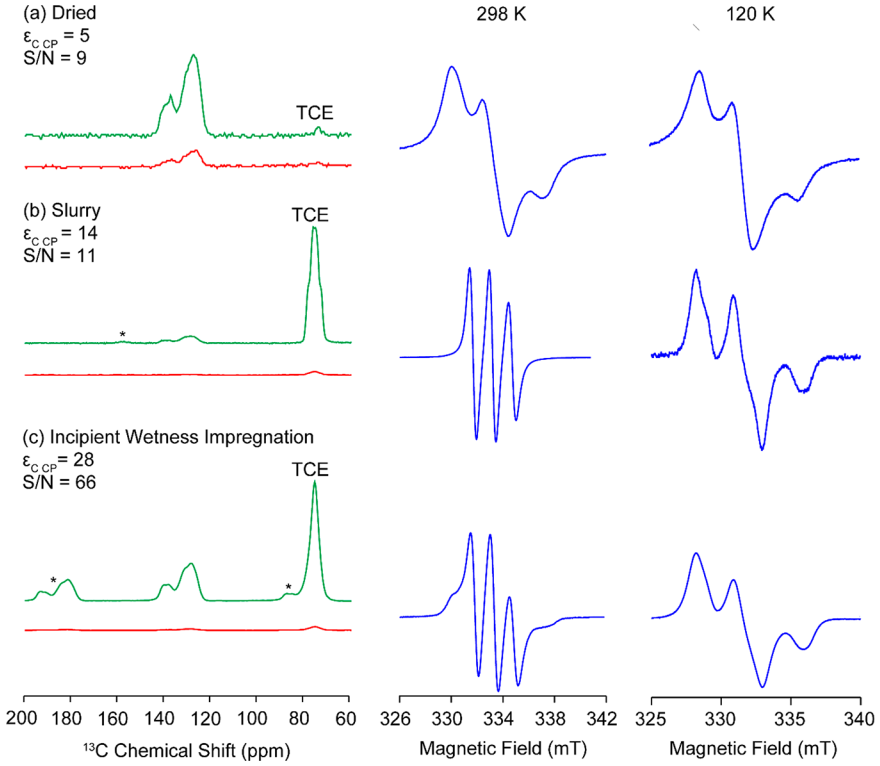

Figure 2. DNP enhanced ^{13}C CP MAS NMR spectra (left) of CP-CMP10 prepared (a) dried (b) as a slurry, and (c) by incipient wetness impregnation at 14.1 T with μw irradiation (green) at $\nu_0(e^-)$ = 395 GHz, and without μw irradiation (red) recorded at 120 K. S/N represents signal-to-noise per unit time ratios of the 110 to 150 ppm region of the spectrum. TCE solvent peaks are labeled in all spectra. The corresponding X-band EPR spectra (blue) are given at room temperature (center) and 120 K (right).

3. RESULTS AND DISCUSSION

Optimizing Sample Preparation. Figure 1 depicts the putative structures of the CP-CMP polymers investigated in this work, postulating that the polymer compositions match the pyrene to benzene ratio of the monomer feed. CP-CMP9 displays reasonable photocatalytic water splitting under visible light, and increasing pyrene concentration in the monomer feed by 25% (CP-CMP10, Figure 1c) leads to a substantial increase in photocatalytic water splitting likely resulting from slight decrease of the optical bandgap. A further 5% increase in monomeric pyrene concentration to CP-CMP11 leads to a sharp decline of photocatalytic activity, and a substantial drop in bandgap. CP-CMP1 and CP-CMP15 show no photocatalytic activity and contain only one polymeric repeat unit (CP-CMP15) or one base benzene unit alternating between di- and tetra-substituted (CP-CMP1).

Figure 2 shows the DNP enhanced ^{13}C CP MAS NMR spectrum of CP-CMP10 using a range of sample preparation approaches for which full details are given in the experimental section, with enhancement given as $\varepsilon_{C\,CP}$ (defined in section S4 of the Supporting Information). Although, film casting has been demonstrated to show excellent DNP enhancement in linear polymers such as polystyrene after dissolution in the radical solution,[39] this method is not practical on CP-CMPs due to their insolubility, and as such other approaches were used. The dried preparation[37] showed a modest signal enhancement in our hands ($\varepsilon_{C\,CP} \sim 5$), while the slurry preparation gave a higher enhancement of $\varepsilon_{C\,CP}$ = 14. For CP-CMP10, incipient wetness impregnation[65] provides the largest $\varepsilon_{C\,CP}$ value (28). This is likely due to a reduction in paramagnetic bleaching due to the lower concentration of radical in the sample[66] and was therefore selected as the optimal sample preparation approach for all CP-CMPs studied here (as shown previously).[67]

EPR of the dried sample (Figure 2a) shows anisotropic line broadening of immobile TEKPol radical likely caused by electron−electron dipolar and/or exchange interactions, whereas the EPR spectrum of the slurry (Figure 2b) is much narrower, indicative of mobile radical. The EPR of CP-CMP10 prepared by incipient wetness impregnation suggests that the radical/solvent solution fills the pores of the polymer lattice (Figure 2c), as revealed by the EPR line shape showing a combination of narrow lines, indicative of TEKPol in solution, with broadened shoulders, illustrating the presence of immobile TEKPol within the polymer.[68] EPR at 120 K, reflective of the temperature at which the DNP experiments would be recorded, showed typical "powder" spectra (Figure 2). The same line shape trends are observed as at room temperature, with the incipient wetness impregnation sample showing a hybrid line shape, between that of the dried sample and the slurry, which represents the free radical in frozen solution. It is possible that the additional broadening observed in the dried sample (and to a lesser extent, incipient wetness impregnation) could be attributed to dipolar broadening and/or weak exchange coupling, however, there is an absence of strong exchange coupling in all preparations.[69] The data therefore suggests that there is no further aggregation of radical occurring at low temperature. EPR spin counting experiment on this sample yielded $(9 \pm 1) \times 10^{17}$ electron spins in reasonable agreement with the $(6 \pm 4) \times 10^{17}$ spins anticipated from the DNP sample preparation procedure. This illustrates the absence of measurable degradation of TEKPol in contact to CP-CMP10.

DOI: 10.1021/acs.macromol.7b02544
Macromolecules 2018, 51, 3088−3096

Spectral Assignment. In order to unequivocally assign the ^{13}C MAS spectrum of CP-CMP10, a 9.4 T DNP enhanced J-based $^{13}C-^{13}C$ correlation spectrum was obtained using the refocused INADEQUATE experiment and yields carbon–carbon connectivities (Figure 3).[70] Despite the inherently very

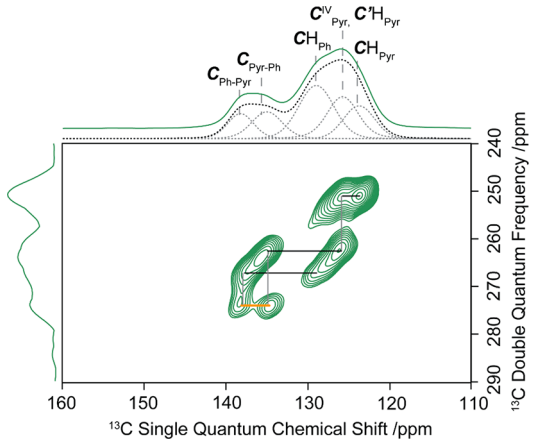

Figure 3. DNP enhanced ^{13}C refocused INADEQUATE MAS NMR spectrum of CP-CMP10 at $\nu_0(^1H)$ = 400.07 MHz with μw on with all correlations assigned (black) and the pyrene-benzene correlation highlighted (orange). Top: DNP enhanced ^{13}C CP MAS NMR spectrum of CP-CMP10 (green) with spectral simulations (black dashed) and peak deconvolutions (gray dashed), left: double quantum INADEQUATE projection.

low sensitivity of this experiment at ^{13}C natural abundance due to the very low probability of having a pair of ^{13}C nuclei (0.01% abundant), the sensitivity enhancement of DNP enables such an experiment to be readily obtained as demonstrated previously.[37,71]

The corresponding 2D spectrum of CP-CMP10 is given in Figure 3 and reveals a clear correlation between the C_{Pyr-Ph} at 136 ppm and the C_{Ph-Pyr} at 138 ppm (shown in orange in Figure 1(c) and 3), confirming the formation of the pyrene-benzene bond and the successful polymerization. Three other correlations were identified (shown in black, Figure 3), allowing full spectral assignment of CP-CMP10 (Figures 3 and 4). The resonances of C^{IV}_{Pyr} and $C'H_{Pyr}$ overlap at 126 ppm, and thus in the second dimension their respective correlations with C_{Pyr-Ph} are also unresolved.

To confirm this assignment, the DNP enhanced ^{13}C CP MAS NMR spectra of the homopolymers CP-CMP1 and CP-CMP15 are given in Figure 4, parts a and e; while the ^{13}C NMR spectrum of the entirely di- or tetra-substituted benzene polymer CP-CMP1 shows two distinct resonances at 138 and 128 ppm (assigned by $^{13}C-^{13}C$ correlation experiment to the quaternary C_{Ph-Ph}, and CH_{Ph} respectively, details given in proceeding paragraphs), the spectrum of homocoupled pyrene, CP-CMP15, displays signals at 134, 128, and 124 ppm that are assigned to $C_{Pyr-Pyr}$, C^{IV}_{Pyr}, $C'H_{Pyr}$, and CH_{Pyr} using a combination of short contact time cross-polarization and previous literature.[72] More importantly, both C_{Ph-Ph} and $C_{Pyr-Pyr}$ quaternary carbons, which are typical of the benzene and pyrene moieties, appear at slightly different shifts, enabling observation of both pyrene and benzene monomers in the CP-CMP9, CP-CMP10, and CP-CMP11 polymers (Figure 4b–d). For example, the ^{13}C spectrum of CP-CMP9 displays both C_{Ph-Pyr} and C_{Pyr-Ph} resonances in addition to three others assigned to protonated carbons (*vide infra*). Note that although

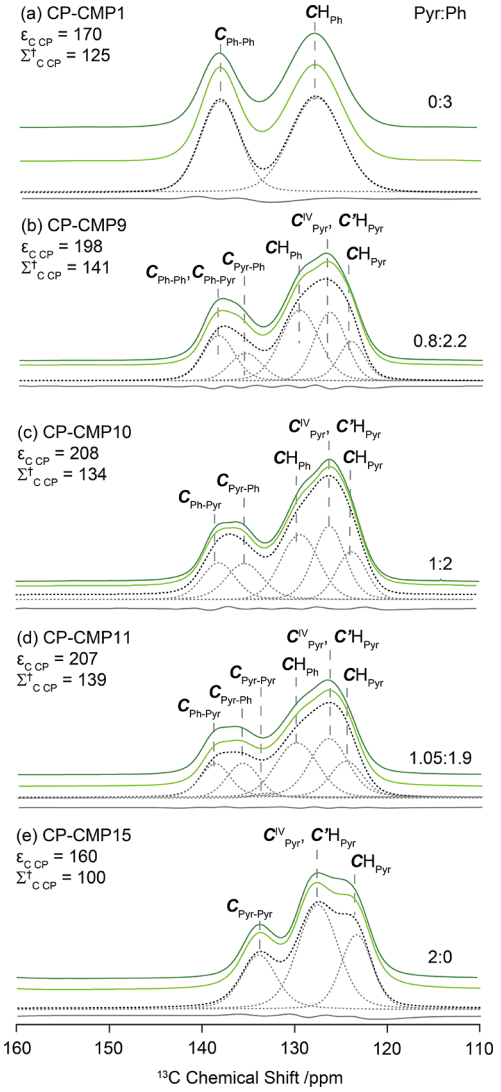

Figure 4. DNP enhanced ^{13}C CP (green) and multiCP (light green) MAS NMR spectra of (a–e) CP-CMP1-15 recorded at $\nu_0(^1H)$ = 400.07 MHz, with μw on (green), simulated (dashed black), spectral deconvolution (dashed gray) and difference between experimental and simulated spectra (solid gray). Left is the ^{13}C DNP enhancement and overall gain, and on the right is the pyrene to benzene unit ratio of the monomer feed.

seven chemically inequivalent carbon environments are anticipated in CP-CMP9, only five ^{13}C NMR signals can be resolved (Figures 3 and 4), likely due to the substantial inhomogeneous line broadening and short T_2' times. All five resolvable resonances of CP-CMP9 are also present in the DNP spectrum of CP-CMP10 albeit with slightly different intensities; this is consistent with a different ratio of the same monomeric units used during synthesis (Table 1, Figure 1). The DNP-enhanced ^{13}C CP MAS NMR spectrum of CP-CMP11 is very similar to those of CP-CMP9 and CP-CMP10, albeit with possibly an additional low intensity resonance at 134 ppm corresponding to a quaternary pyrene carbon directly bonded to another pyrene molecule ($C_{Pyr-Pyr}$); based on the monomer feed ratio this signal should only be present in one out of every 20 polymeric repeat units. Despite the inherent low intensity of this peak, it is observable within 20 min with DNP, and deconvolution of these spectra allows visualization of these changes with respect to the monomer feed (Figure 4).

DOI: 10.1021/acs.macromol.7b02544
Macromolecules 2018, 51, 3088–3096

Quantifying Enhancement Using Overall DNP Gain Factor $\Sigma^{\dagger}$. In order to better reflect on the large enhancements observed, an overall DNP gain factor, $\Sigma^{\dagger}_{C\ CP}$ was also calculated (Table S2).[37,71,73,74] $\Sigma^{\dagger}$ is a comparison of the ^{13}C DNP enhanced spectrum vs a standard 400 MHz NMR spectrum obtained at room temperature, a full discussion of which is beyond the scope of this work and is provided elsewhere.[37,71,73−75] $\Sigma^{\dagger}$ compensates for weight, and accounts for time saving, signal bleaching due to introduction of paramagnetic radicals and temperature differences, and estimates the overall benefit of DNP (see section S4 of the Supporting Information to calculate these values). The $\Sigma^{\dagger}_{C\ CP}$ values determined for CP-CMP9, CP-CMP10, and CP-CMP11 are all around 140, showing time efficient acquisition of high signal-to-noise ^{13}C NMR spectra. The $\Sigma^{\dagger}_{C\ CP}$ values for CP-CMP1 and CP-CMP15 were a little lower than for the copolymers, a similar trend to that observed for their $\varepsilon_{C\ CP}$. Although, this disparity is not immediately attributable to any one physical property (such as SA_{BET}), the two homopolymers are significantly different systems from the copolymers, and the result is reproducible. Note that there is a large paramagnetic bleaching effect (θ values between 0.2 and 0.4, Table S1); the large surface area of these materials offers intimate distribution of radical leading to a greater bleaching, although the signal bleaching is constant within a monomeric unit of the polymer.

DNP MultiCP at 400 MHz. While the DNP-enhanced ^{13}C CP MAS NMR spectra of selected CP-CMPs confirm that the final macromolecular structure is directly related to monomer feed ratio, quantitative data are needed to determine the polymer compositions and were obtained by recording ^{13}C multiCP DNP NMR experiments.[46−49]

This methodology provides a robust quantification approach[51] that is also time efficient (versus alternative methods such variable contact times CP experiments) and allows assignment of polymeric structure which can be cross checked with monomer feed ratio (Table 2). It has previously been reported that the enhancement of DNP can appear nonuniform in heterogeneous systems, due to microwave induced sample heating and temperature dependent relaxation times.[41] In the CP-CMP systems we investigated, the DNP enhancements observed are homogeneous throughout the ^{13}C NMR spectra (Figure S6) due to the similar environments and relaxation times of all carbon resonances as well as the porosity of the materials leading to radical distribution throughout the system, facilitating $^{1}H-^{1}H$ spin diffusion for homogeneous polarization transfer. The polymers studied met all conditions for the multiCP spectra as given in previous work ($\tau_{DNP}(^{13}C)$ greatly exceeded 500 s as shown in Figure S7, satisfying $\tau_{DNP}(^{13}C) > 10 \times \tau_{DNP}(^{1}H)$, contact time <10% $T_{1\rho}(^{1}H)$),[49,51] a full discussion of which can be found in section S5 of the Supporting Information.

Table 2. Monomer Feed Ratios and DNP ^{13}C MultiCP Integration of the Repeat Units within CP-CMP1, CP-CMP9, CP-CMP10, CP-CMP11, and CP-CMP15

	monomer feed		measured ratios[a]	
polymer	pyrene	benzene	pyrene	benzene
CP-CMP1	0	3	0	3.1 ± 0.3
CP-CMP9	0.8	2.2	0.8 ± 0.1	2.3 ± 0.2
CP-CMP10	1	2	1.0 ± 0.1	1.9 ± 0.2
CP-CMP11	1.05	1.9	1.02 ± 0.1	1.9 ± 0.2
CP-CMP15	2	0	2.1 ± 0.2	0

[a]Ratios calculated from the sum integration of all resonances of each monomer (Table S3), divided by the number of carbon atoms per monomer unit.

The DNP enhanced ^{13}C multiCP MAS NMR spectra of CP-CMP1−15 are shown in Figure 4, parts a−e, alongside the spectral simulation and difference between experimental and simulated data, while Table 2 provides a comparison between the predicted carbons ratio based on the monomers feed with the ^{13}C NMR data integration (examples of the full spectral fit can be found in Figure S8). The difference in integration between multiCP and CP spectra can be found in Table S3. Both homopolymers CP-CMP1 and CP-CMP15 were quantified using DNP multiCP (Figure 4, parts a and e) as an internal standard, both showing integrations closely matching their theoretical ratios from monomer feed (Table 2). As the covalent geometry of both benzene and pyrene are known, the relative integration ratios of resonances were fixed to one another for deconvolution purposes, in order to elucidate the relative stoichiometry of benzene to pyrene more accurately.

In CP-CMP10, the equal stoichiometry of pyrene and benzene monomers reported in Table 2 is readily visualized by the equal integration of $C_{Ph\text{-}Pyr}$ (138 ppm) and $C_{Pyr\text{-}Ph}$ (136 ppm). The integration ratios of the pyrene compared to the benzene resonances obtained in CP-CMP9 matches the monomer feed (Table 2), notably showing the greater integration of the $C_{Ph\text{-}Pyr}/C_{Ph\text{-}Ph}$ signal (138 ppm) compared to the $C_{Pyr\text{-}Ph}$ peak (at 136 ppm) and representing a larger concentration of benzene than pyrene units in the polymer network.

The multiCP spectrum of CP-CMP11 also shows that the unique $C_{Pyr\text{-}Pyr}$ carbon environment in this polymer (134 ppm) integrates consistently with a pyrene−pyrene component being present on average once in every 20 repeat units. From the full polymeric assignments made possible by the INADEQUATE spectrum, it was possible to relate the final structures with the monomer ratio and, within error, showing stoichiometric uptake of each monomer, giving a polymer network that reflects the feed ratio.

4. CONCLUSION

We have demonstrated that DNP permits the fast acquisition of high signal-to-noise ratio ^{13}C CP MAS NMR spectra of amorphous polymeric networks assembled from pyrene and benzene units and enables the observation of carbon environments that appear rarely in the repeating units (e.g., once in every 20). The gain of sensitivity allows natural abundance $^{13}C-^{13}C$ correlation spectra of these amorphous polymers to be obtained, facilitating the ^{13}C NMR spectra assignments. DNP combined with the multiCP approach enabled quantitative ^{13}C NMR spectra to be recorded and yield the polymers' compositions which compare well with the monomer feed ratio. This work establishes the polymer composition and allows trends in band gap[8] to be directly related to the polymeric structure rather than inferring this from the monomers feed.

■ ASSOCIATED CONTENT

Supporting Information

The Supporting Information is available free of charge on the ACS Publications website at DOI: 10.1021/acs.macro-

DOI: 10.1021/acs.macromol.7b02544
Macromolecules 2018, 51, 3088−3096

mol.7b02544. The raw data of each figure shown in this work are provided as a supporting dataset, available from the University of Liverpool Data Catalogue portal http://data-cat.liverpool.ac.uk/451/.

Details of porosity and surface area measurements, NMR experiments used, PXRD, overall sensitivity enhancement factor $\Sigma^{\dagger}$ calculations, multiCP parameters, and additional figures (PDF)

AUTHOR INFORMATION

Corresponding Author

*(F.B.) E-mail: frederic.blanc@liverpool.ac.uk.

ORCID

Alistair J. Fielding: 0000-0002-4437-9791

Andrew I. Cooper: 0000-0003-0201-1021

Frédéric Blanc: 0000-0001-9171-1454

Funding

Financial support from the EPSRC for Doctoral Training Studentships (to N.J.B.), Grants EP/N004884/1 (to R.S.S. and A.I.C.) and EP/M00869X/1 (to F.B.) are acknowledged. A.J.F. thanks Bruker for funding.

Notes

The authors declare no competing financial interest.

ACKNOWLEDGMENTS

We thank Dr. Werner E. Maas for allowing access to the Bruker DNP Demo Laboratories in Billerica and Wissembourg. An allocation of time at the National EPR Facility and Service, Photon Sciences Institute, The University of Manchester, which is funded by the EPSRC is acknowledged, and Mr. Adam Brookfield is thanked for valuable technical assistance. Dr. Olivier Ouari and Prof. Paul Tordo are acknowledged for providing radicals, and we thank Dr. Ivan Sergeyev and Mr. Leo Tometich for valuable technical assistance.

REFERENCES

(1) Kudo, A.; Miseki, Y.; Uetsuda, H.; Onishi, H.; Morton, O.; Torimoto, T.; Kudo, A.; Kuwabata, S.; Domen, K.; Li, C.; Domen, K.; Lee, C. Heterogeneous Photocatalyst Materials for Water Splitting. *Chem. Soc. Rev.* **2009**, *38*, 253−278.

(2) Chen, X.; Shen, S.; Guo, L.; Mao, S. S. Semiconductor-Based Photocatalytic Hydrogen Generation. *Chem. Rev.* **2010**, *110*, 6503−6570.

(3) Wang, Q.; Hisatomi, T.; Jia, Q.; Tokudome, H.; Zhong, M.; Wang, C.; Pan, Z.; Takata, T.; Nakabayashi, M.; Shibata, N.; Li, Y.; Sharp, I. D.; Kudo, A.; Yamada, T.; Domen, K. Scalable Water Splitting on Particulate Photocatalyst Sheets with a Solar-to-Hydrogen Energy Conversion Efficiency Exceeding 1%. *Nat. Mater.* **2016**, *15*, 611−615.

(4) Wang, X.; Maeda, K.; Thomas, A.; Takanabe, K.; Xin, G.; Carlsson, J. M.; Domen, K.; Antonietti, M. A Metal-Free Polymeric Photocatalyst for Hydrogen Production from Water under Visible Light. *Nat. Mater.* **2009**, *8*, 76−80.

(5) Yanagida, S.; Kabumoto, A.; Mizumoto, K.; Pac, C.; Yoshino, K. Poly(p-Phenylene)-Catalysed Photoreduction of Water to Hydrogen. *J. Chem. Soc., Chem. Commun.* **1985**, *0*, 474−475.

(6) Shibata, T.; Kabumoto, A.; Shiragami, T.; Ishitani, O.; Pac, C.; Yanagida, S. Novel Visible-Light-Driven Photocatalyst. Poly(p-Phenylene)-Catalyzed Photoreductions of Water, Carbonyl Compounds, and Olefins. *J. Phys. Chem.* **1990**, *94*, 2068−2076.

(7) Sprick, R. S.; Bonillo, B.; Clowes, R.; Guiglion, P.; Brownbill, N. J.; Slater, B. J.; Blanc, F.; Zwijnenburg, M. A.; Adams, D. J.; Cooper, A. I. Visible-Light-Driven Hydrogen Evolution Using Planarized Conjugated Polymer Photocatalysts. *Angew. Chem., Int. Ed.* **2016**, *55*, 1792−1796.

(8) Sprick, R. S.; Jiang, J.-X.; Bonillo, B.; Ren, S.; Ratvijitvech, T.; Guiglion, P.; Zwijnenburg, M. A.; Adams, D. J.; Cooper, A. I. Tunable Organic Photocatalysts for Visible-Light-Driven Hydrogen Evolution. *J. Am. Chem. Soc.* **2015**, *137*, 3265−3270.

(9) Vyas, V. S.; Haase, F.; Stegbauer, L.; Savasci, G.; Podjaski, F.; Ochsenfeld, C.; Lotsch, B. V. A Tunable Azine Covalent Organic Framework Platform for Visible Light-Induced Hydrogen Generation. *Nat. Commun.* **2015**, *6*, 8508.

(10) Li, L.; Cai, Z.; Wu, Q.; Lo, W.-Y.; Zhang, N.; Chen, L. X.; Yu, L. Rational Design of Porous Conjugated Polymers and Roles of Residual Palladium for Photocatalytic Hydrogen Production. *J. Am. Chem. Soc.* **2016**, *138*, 7681−7686.

(11) Yang, C.; Ma, B. C.; Zhang, L.; Lin, S.; Ghasimi, S.; Landfester, K.; Zhang, K. A. I.; Wang, X. Molecular Engineering of Conjugated Polybenzothiadiazoles for Enhanced Hydrogen Production by Photosynthesis. *Angew. Chem., Int. Ed.* **2016**, *55*, 9202−9206.

(12) Li, L.; Hadt, R. G.; Yao, S.; Lo, W.-Y.; Cai, Z.; Wu, Q.; Pandit, B.; Chen, L. X.; Yu, L. Photocatalysts Based on Cobalt-Chelating Conjugated Polymers for Hydrogen Evolution from Water. *Chem. Mater.* **2016**, *28*, 5394−5399.

(13) Sprick, R. S.; Bonillo, B.; Sachs, M.; Clowes, R.; Durrant, J. R.; Adams, D. J.; Cooper, A. I. Extended Conjugated Microporous Polymers for Photocatalytic Hydrogen Evolution from Water. *Chem. Commun.* **2016**, *52*, 10008−10011.

(14) Wang, L.; Fernández-Terán, R.; Zhang, L.; Fernandes, D. L. A.; Tian, L.; Chen, H.; Tian, H. Organic Polymer Dots as Photocatalysts for Visible Light-Driven Hydrogen Generation. *Angew. Chem., Int. Ed.* **2016**, *55*, 12306−12310.

(15) Li, L.; Lo, W.; Cai, Z.; Zhang, N.; Yu, L. Donor−Acceptor Porous Conjugated Polymers for Photocatalytic Hydrogen Production: The Importance of Acceptor Comonomer. *Macromolecules* **2016**, *49*, 6903−6909.

(16) Bi, S.; Lan, Z.-A.; Paasch, S.; Zhang, W.; He, Y.; Zhang, C.; Liu, F.; Wu, D.; Zhuang, X.; Brunner, E.; Wang, X.; Zhang, F. Substantial Cyano-Substituted Fully Sp^2 -Carbon-Linked Framework: Metal-Free Approach and Visible-Light-Driven Hydrogen Evolution. *Adv. Funct. Mater.* **2017**, *27*, 1703146.

(17) Woods, D. J.; Sprick, R. S.; Smith, C. L.; Cowan, A. J.; Cooper, A. I. A Solution-Processable Polymer Photocatalyst for Hydrogen Evolution from Water. *Adv. Energy Mater.* **2017**, *7*, 1700479.

(18) Cooper, A. I. Conjugated Microporous Polymers. *Adv. Mater.* **2009**, *21*, 1291−1295.

(19) Schmidt-Rohr, K.; Spiess, H. W. *Multidimensional Solid-State NMR and Polymers*; Academic Press: London, 1994.

(20) Cheng, H. N.; Asakura, T.; English, A. D. *NMR Spectroscopy of Polymers: Innovative Strategies for Complex Macromolecules*; American Chemical Society: Washington DC, 2011.

(21) Jiang, J.-X.; Li, Y.; Wu, X.; Xiao, J.; Adams, D. J.; Cooper, A. I. Conjugated Microporous Polymers with Rose Bengal Dye for Highly Efficient Heterogeneous Organo-Photocatalysis. *Macromolecules* **2013**, *46*, 8779−8783.

(22) Bonillo, B.; Sprick, S.; Cooper, A. I. Tuning Photophysical Properties in Conjugated Microporous Polymers by Comonomer Doping Strategies. *Chem. Mater.* **2016**, *28*, 3469−3480.

(23) Wei, G.; Basheer, C.; Tan, C.-H.; Jiang, Z. Visible Light Photocatalysis in Chemoselective Functionalization of C(sp3)H Bonds Enabled by Organic Dyes. *Tetrahedron Lett.* **2016**, *57*, 3801−3809.

(24) Pines, A.; Gibby, M. G.; Waugh, J. S. Proton-Enhanced Nuclear Induction Spectroscopy 13C Chemical Shielding Anisotropy in Some Organic Solids. *Chem. Phys. Lett.* **1972**, *15*, 373−376.

(25) Overhauser, A. W. Polarization of Nuclei in Metals. *Phys. Rev.* **1953**, *92*, 411−415.

(26) Carver, T. R.; Slichter, C. P. Experimental Verification of the Overhauser Nuclear Polarization Effect. *Phys. Rev.* **1956**, *102*, 975−980.

(27) Hall, D. A.; Maus, D. C.; Gerfen, G. J.; Inati, S. J.; Becerra, L. R.; Dahlquist, F. W.; Griffin, R. G. Polarization-Enhanced NMR Spectroscopy of Biomolecules in Frozen Solution. *Science* **1997**, *276*, 930−932.

DOI: 10.1021/acs.macromol.7b02544
Macromolecules 2018, 51, 3088−3096

(28) Ni, Q. Z.; Daviso, E.; Can, T. V.; Markhasin, E.; Jawla, S. K.; Swager, T. M.; Temkin, R. J.; Herzfeld, J.; Griffin, R. G. High Frequency Dynamic Nuclear Polarization. *Acc. Chem. Res.* **2013**, *46*, 1933−1941.
(29) Hwang, C. F.; Hill, D. A. New Effect In Dynamic Polarisation. *Phys. Rev. Lett.* **1967**, *18*, 110−112.
(30) Hwang, C. F.; Hasher, B. A.; Hill, D. A.; Markley, F. The Use of Chemically Doped Polystyrene as a Polarized Proton Target Material. *Nucl. Instrum. Methods* **1967**, *51*, 254−256.
(31) Afeworki, M.; McKay, R. A.; Schaefer, J. Selective Observation of the Interface of Heterogeneous Polycarbonate/polystyrene Blends by Dynamic Nuclear Polarization Carbon-13 NMR Spectroscopy. *Macromolecules* **1992**, *25*, 4084−4091.
(32) Afeworki, M.; Schaefer, J. Mechanism of DNP-Enhanced Polarization Transfer across the Interface of Polycarbonate/polystyrene Heterogeneous Blends. *Macromolecules* **1992**, *25*, 4092−4096.
(33) Afeworki, M.; McKay, R. A.; Schaefer, J. Dynamic Nuclear Polarization Enhanced Nuclear Magnetic Resonance of Polymer-Blend Interfaces. *Mater. Sci. Eng., A* **1993**, *162*, 221−228.
(34) Wind, R. A.; Zumbulyadis, N.; Young, R. H.; Hung, Y.; Li, L.; Nuttall, R. H. D.; Maciel, G. EPR and 1H and 13C Dynamic Nuclear Polarization Studies of a Molecularly Doped Polymer: Bisphenol A Polycarbonate Doped with Trianisylamine and Trianisylaminium Perchlorate. *Solid State Nucl. Magn. Reson.* **1992**, *1*, 55−65.
(35) Wind, R. A.; Duijvestijn, M. J.; van der Lugt, C.; Manenschijn, A.; Vriend, J. Applications of Dynamic Nuclear Polarization in 13C NMR in Solids. *Prog. Nucl. Magn. Reson. Spectrosc.* **1985**, *17*, 33−67.
(36) Horii, F.; Idehara, T.; Fujii, Y.; Ogawa, I.; Horii, A.; Entzminger, G.; Doty, F. D. Development of DNP-Enhanced High-Resolution Solid-State NMR System for the Characterization of the Surface Structure of Polymer Materials. *J. Infrared, Millimeter, Terahertz Waves* **2012**, *33*, 756−765.
(37) Takahashi, H.; Lee, D.; Dubois, L.; Bardet, M.; Hediger, S.; De Paëpe, G. Rapid Natural-Abundance 2D ^{13}C-^{13}C Correlation Spectroscopy Using Dynamic Nuclear Polarization Enhanced Solid-State NMR and Matrix-Free Sample Preparation. *Angew. Chem., Int. Ed.* **2012**, *51*, 11766−11769.
(38) Ouari, O.; Phan, T.; Ziarelli, F.; Casano, G.; Aussenac, F.; Thureau, P.; Gigmes, D.; Tordo, P.; Viel, S. Improved Structural Elucidation of Synthetic Polymers by Dynamic Nuclear Polarization Solid-State NMR Spectroscopy. *ACS Macro Lett.* **2013**, *2*, 715−719.
(39) Le, D.; Casano, G.; Phan, T. N. T.; Ziarelli, F.; Ouari, O.; Aussenac, F.; Thureau, P.; Mollica, G.; Gigmes, D.; Tordo, P.; Viel, S. Optimizing Sample Preparation Methods for Dynamic Nuclear Polarization Solid-State NMR of Synthetic Polymers. *Macromolecules* **2014**, *47*, 3909−3916.
(40) Le, D.; Ziarelli, F.; Phan, T. N. T.; Mollica, G.; Thureau, P.; Aussenac, F.; Ouari, O.; Gigmes, D.; Tordo, P.; Viel, S. Up to 100% Improvement in Dynamic Nuclear Polarization Solid-State NMR Sensitivity Enhancement of Polymers by Removing Oxygen. *Macromol. Rapid Commun.* **2015**, *36*, 1416−1421.
(41) Mollica, G.; Le, D.; Ziarelli, F.; Casano, G.; Ouari, O.; Phan, T. N. T.; Aussenac, F.; Thureau, P.; Gigmes, D.; Tordo, P.; Viel, S. Observing Apparent Nonuniform Sensitivity Enhancements in Dynamic Nuclear Polarization Solid-State NMR Spectra of Polymers. *ACS Macro Lett.* **2014**, *3*, 922−925.
(42) Blanc, F.; Chong, S. Y.; McDonald, T. O.; Adams, D. J.; Pawsey, S.; Caporini, M. A.; Cooper, A. I. Dynamic Nuclear Polarization NMR Spectroscopy Allows High-Throughput Characterization of Microporous Organic Polymers. *J. Am. Chem. Soc.* **2013**, *135*, 15290−15293.
(43) Chaudhari, S. R.; Griffin, J. M.; Broch, K.; Lesage, A.; Lemaur, V.; Dudenko, D.; Olivier, Y.; Sirringhaus, H.; Emsley, L.; Grey, C. P. Donor−acceptor Stacking Arrangements in Bulk and Thin-Film High-Mobility Conjugated Polymers Characterized Using Molecular Modelling and MAS and Surface-Enhanced Solid-State NMR Spectroscopy. *Chem. Sci.* **2017**, *8*, 3126−3136.
(44) Perras, F. A.; Luo, H.; Zhang, X.; Mosier, N. S.; Pruski, M.; Abu-Omar, M. M. Atomic-Level Structure Characterization of Biomass Pre- and Post- Lignin Treatment by Dynamic Nuclear Polarization-Enhanced Solid- State NMR. *J. Phys. Chem. A* **2017**, *121*, 623−630.
(45) Maly, T.; Miller, A.-F.; Griffin, R. G. In Situ High-Field Dynamic Nuclear Polarization-Direct and Indirect Polarization of 13C Nuclei. *ChemPhysChem* **2010**, *11*, 999−1001.
(46) Zhang, S.; Wu, X.; Mehring, M. Successive Polarization under Mismatched Hartmann—Hahn Condition. *Chem. Phys. Lett.* **1990**, *166*, 92−94.
(47) Nevzorov, A. A. Ergodicity and Efficiency of Cross-Polarization in NMR of Static Solids. *J. Magn. Reson.* **2011**, *209*, 161−166.
(48) Raya, J.; Perrone, B.; Hirschinger, J. Chemical Shift Powder Spectra Enhanced by Multiple-Contact Cross-Polarization under Slow Magic-Angle Spinning. *J. Magn. Reson.* **2013**, *227*, 93−102.
(49) Johnson, R. L.; Schmidt-Rohr, K. Quantitative Solid-State 13C NMR with Signal Enhancement by Multiple Cross Polarization. *J. Magn. Reson.* **2014**, *239*, 44−49.
(50) Monti, G. A.; Chattah, A. K.; Linck, Y. G. *Annu. Rep. NMR Spectrosc.* **2014**, *83*, 221−269.
(51) Saïdi, F.; Taulelle, F.; Martineau, C. Quantitative 13C Solid-State NMR Spectra by Multiple-Contact Cross-Polarization for Drug Delivery: From Active Principles to Excipients and Drug Carriers. *J. Pharm. Sci.* **2016**, *105*, 2397−2401.
(52) Johnson, R. L.; Perras, F. A.; Kobayashi, T.; Schwartz, T. J.; Dumesic, J. A.; Shanks, B. H.; Pruski, M. Identifying Low-Coverage Surface Species on Supported Noble Metal Nanoparticle Catalysts by DNP-NMR. *Chem. Commun.* **2016**, *52*, 1859−1862.
(53) Hu, K.-N.; Song, C.; Yu, H.; Swager, T. M.; Griffin, R. G. High-Frequency Dynamic Nuclear Polarization Using Biradicals: A Multifrequency EPR Lineshape Analysis. *J. Chem. Phys.* **2008**, *128*, 052302.
(54) Miyaura, N.; Suzuki, A. Palladium-Catalyzed Cross-Coupling Reactions of Organoboron Compounds. *Chem. Rev.* **1995**, *95*, 2457−2483.
(55) Zagdoun, A.; Casano, G.; Ouari, O.; Schwarzwälder, M.; Rossini, A. J.; Aussenac, F.; Yulikov, M.; Jeschke, G.; Copéret, C.; Lesage, A.; Tordo, P.; Emsley, L. Large Molecular Weight Nitroxide Biradicals Providing Efficient Dynamic Nuclear Polarization at Temperatures up to 200 K. *J. Am. Chem. Soc.* **2013**, *135*, 12790−12797.
(56) Zagdoun, A.; Rossini, A. J.; Gajan, D.; Bourdolle, A.; Ouari, O.; Rosay, M.; Maas, W. E.; Tordo, P.; Lelli, M.; Emsley, L.; Lesage, A.; Copéret, C. Non-Aqueous Solvents for DNP Surface Enhanced NMR Spectroscopy. *Chem. Commun.* **2012**, *48*, 654−656.
(57) Kubicki, D. J.; Rossini, A. J.; Purea, A.; Zagdoun, A.; Ouari, O.; Tordo, P.; Engelke, F.; Lesage, A.; Emsley, L. Amplifying Dynamic Nuclear Polarization of Frozen Solutions by Incorporating Dielectric Particles. *J. Am. Chem. Soc.* **2014**, *136*, 15711−15718.
(58) Matsuki, Y.; Takahashi, H.; Ueda, K.; Idehara, T.; Ogawa, I.; Toda, M.; Akutsu, H.; Fujiwara, T. Dynamic Nuclear Polarization Experiments at 14.1 T for Solid-State NMR. *Phys. Chem. Chem. Phys.* **2010**, *12*, 5799−5803.
(59) Song, C.; Hu, K.-N.; Joo, C.-G.; Swager, T. M.; Griffin, R. G. TOTAPOL: A Biradical Polarizing Agent for Dynamic Nuclear Polarization Experiments in Aqueous Media. *J. Am. Chem. Soc.* **2006**, *128*, 11385−11390.
(60) Thurber, K. R.; Tycko, R. Measurement of Sample Temperatures under Magic-Angle Spinning from the Chemical Shift and Spin-Lattice Relaxation Rate of 79Br in KBr Powder. *J. Magn. Reson.* **2009**, *196*, 84−87.
(61) Fung, B. M.; Khitrin, A. K.; Ermolaev, K. An Improved Broadband Decoupling Sequence for Liquid Crystals and Solids. *J. Magn. Reson.* **2000**, *142*, 97−101.
(62) Rosay, M.; Tometich, L.; Pawsey, S.; Bader, R.; Schauwecker, R.; Blank, M.; Borchard, P. M.; Cauffman, S. R.; Felch, K. L.; Weber, R. T.; Temkin, R. J.; Griffin, R. G.; Maas, W. E. Solid-State Dynamic Nuclear Polarization at 263 GHz: Spectrometer Design and Experimental Results. *Phys. Chem. Chem. Phys.* **2010**, *12*, 5850−5860.
(63) Ernst, R. R.; Bodenhausen, G.; Wokaun, A. *Principles of Nuclear Magnetic Resonance in One and Two Dimensions*; Bernstein, R. B., Breslow, R., Green, M. L. H., Halpern, J., Rowlinson, J. L., Eds.; Oxford University Press: 1987.

DOI: 10.1021/acs.macromol.7b02544
Macromolecules 2018, 51, 3088−3096

(64) Morcombe, C. R.; Zilm, K. W. Chemical Shift Referencing in MAS Solid State NMR. *J. Magn. Reson.* **2003**, *162*, 479−486.
(65) Lesage, A.; Lelli, M.; Gajan, D.; Caporini, M. A.; Vitzthum, V.; Miéville, P.; Alauzun, J.; Roussey, A.; Thieuleux, C.; Mehdi, A.; Bodenhausen, G.; Coperet, C.; Emsley, L. Surface Enhanced NMR Spectroscopy by Dynamic Nuclear Polarization. *J. Am. Chem. Soc.* **2010**, *132*, 15459−15461.
(66) Apperley, D. C.; Harris, R. K.; Hodgkinson, P. Relaxation, Exchange and Quantitation. In *Solid-State NMR Basic Principles and Practice*; Momentum Press: New York, 2012; p 212.
(67) Rossini, A. J.; Zagdoun, A.; Lelli, M.; Lesage, A.; Copéret, C.; Emsley, L. Dynamic Nuclear Polarization Surface Enhanced NMR Spectroscopy. *Acc. Chem. Res.* **2013**, *46*, 1942−1951.
(68) Lund, A.; Hsieh, M.-F.; Siaw, T.-A.; Han, S.-I. Direct Dynamic Nuclear Polarization Targeting Catalytically Active 27 Al Sites. *Phys. Chem. Chem. Phys.* **2015**, *17*, 25449−25454.
(69) Bencini, A.; Gatteschi, D. *EPR of Exchange Coupled Systems*; Dove Publications Inc.: 2012.
(70) Lesage, A.; Bardet, M.; Emsley, L. Through-Bond Carbon-Carbon Connectivities in Disordered Solids by NMR. *J. Am. Chem. Soc.* **1999**, *121*, 10987−10993.
(71) Rossini, A. J.; Zagdoun, A.; Hegner, F.; Schwarzwälder, M.; Gajan, D.; Copéret, C.; Lesage, A.; Emsley, L. Dynamic Nuclear Polarization NMR Spectroscopy of Microcrystalline Solids. *J. Am. Chem. Soc.* **2012**, *134*, 16899−16908.
(72) Zwijnenburg, M. A.; Cheng, G.; McDonald, T. O.; Jelfs, K. E.; Jiang, J.-X.; Ren, S.; Hasell, T.; Blanc, F.; Cooper, A. I.; Adams, D. J. Shedding Light on Structure−Property Relationships for Conjugated Microporous Polymers: The Importance of Rings and Strain. *Macromolecules* **2013**, *46*, 7696−7704.
(73) Thurber, K. R.; Yau, W.-M.; Tycko, R. Low-Temperature Dynamic Nuclear Polarization at 9.4 T with a 30 mW Microwave Source. *J. Magn. Reson.* **2010**, *204*, 303−313.
(74) Rossini, A. J.; Zagdoun, A.; Lelli, M.; Gajan, D.; Rascón, F.; Rosay, M.; Maas, W. E.; Copéret, C.; Lesage, A.; Emsley, L. One Hundred Fold Overall Sensitivity Enhancements for Silicon-29 NMR Spectroscopy of Surfaces by Dynamic Nuclear Polarization with CPMG Acquisition. *Chem. Sci.* **2012**, *3*, 108−115.
(75) Brownbill, N. J.; Gajan, D.; Lesage, A.; Emsley, L.; Blanc, F. Oxygen-17 Dynamic Nuclear Polarisation Enhanced Solid-State NMR Spectroscopy at 18.8 T. *Chem. Commun.* **2017**, *53*, 2563−2566.

DOI: 10.1021/acs.macromol.7b02544
Macromolecules 2018, 51, 3088−3096